

# Scanning Fabry-Pérot observations of the HH 7-11 outflow system<sup>\*</sup>

T.A. Movsessian<sup>1</sup>, T.Yu. Magakian<sup>1</sup>, P. Amram<sup>2</sup>, J. Boulesteix<sup>2</sup>, and J.-L. Gach<sup>2</sup>

<sup>1</sup> Byurakan Astrophysical Observatory, 378433 Aragatsotn reg., Armenia and Isaac Newton Institute Armenian Branch (tigmov@bao.sci.am; tigmag@sci.am)

<sup>2</sup> Observatoire de Marseille, 2 place Le Verrier, 13248 Marseille Cedex 4, France

Received 7 June 2000 / Accepted 4 October 2000

**Abstract.** Results of Fabry-Pérot scanning interferometry of the HH 7-11 complex of Herbig-Haro objects are presented. Line profiles and velocity fields are derived. In HH 7 and HH 11 morphological changes in various velocities are discovered, which are interpreted as spatially separated bow shocks and Mach disks. Several arcuate-shaped features, oriented in the direction of the outflow, are pointed out. To explain the nature of the difference in the physical parameters of HH 11 and other knots a suggestion is made about the probable intersection of the two outflows.

**Key words:** ISM: individual objects: HH 7-11 – ISM: jets and outflows – ISM: kinematics and dynamics

## 1. Introduction

Herbig-Haro (HH) objects represent regions of shocked excitation, which are being formed by the interaction of supersonic flows with the ambient medium. Some are bow-shaped and associated with the heads of stellar jets (HH 1, HH 34, HH 47; see Mundt et al. 1987). These regions are called the “working surfaces” of the flow (Blandford & Rees 1974), and consist of two shock systems: a bow shock, where the ambient gas accelerates and excites, and an inner shock or Mach disk, where the jet material decelerates (Raga 1988; Blondin et al. 1989). Narrow band imagery (Reipurth & Heathcote 1992) and Fabry-Pérot area spectrophotometry (Morse et al. 1992, 1993, 1994) have shown that it is possible to distinguish the Mach disk emission from the bow shock emission in HH objects, as predicted by Hartigan (1989a).

HH objects very often form chains and multiple bow shocks along the outflow. Such outflows as HH 46/47 (Reipurth & Heathcote 1991, and references therein), HH 34 (Reipurth & Heathcote 1992), or HH 234 (Movsessian 1992; Magakian & Movsessian 1997) can be considered as typical cases. This suggests that outflows from young stellar objects are non-steady,

and investigation of such systems probes the outflow time history. Sometimes, when several outflows occur in the same region, a whole “nest” of flow sources have been observed. The best examples are the HL/XZ Tau (Mundt et al. 1990) and HH 24 (Eisloffel & Mundt 1997) regions. A detailed study of spectral and morphological characteristics in such groups by standard methods could be very time-consuming. On the other hand, the application of Fabry-Pérot (FP) area spectrophotometry to the analysis of large HH objects and groups is very useful as it offers the possibility to study the spatially resolved velocity field and the profiles of emission lines with high resolution in the whole area. The images restored from FP data have enhanced contrast due to the narrow bandpass of the interferometer. This allows to detect emission nebulosities superposed on a background with bright continuum (see e.g. Magakian et al. 1994). Furthermore, it is possible to reveal the subtle kinematical and morphological details, which are not seen in integrated light or with narrow band filter imaging.

The HH 7-11 group of HH objects is located in the NGC 1333 region, where a “burst” of HH flows was recently discovered (Bally et al. 1996) indicating that violent star formation has been taking place there. This group was found by Herbig (1974) and then became the subject of many studies at optical, radio and infrared wavelengths. One of the most interesting features of this system is its very low excitation (Böhm et al. 1980, 1983), combined with rather high velocities. Up to now, the most thorough morphological and kinematical study of this group was performed by Solf & Böhm (SB) (1987). They found many interesting features, such as radial velocity gradients in the separate knots, variations in the excitation, density and velocity dispersion between individual HH objects, but also concluded that there are no good scenarios to explain more or less consistently all features of this system. Especially difficult is the case of HH 11, where the rather high velocity is associated with a very low excitation and the lack of H<sub>2</sub> emission (Hartigan et al. 1989b), recently confirmed by new observations (Molinari et al. 2000). Another interesting feature is that HH 11 is the only object in the group with detectable proper motion (Herbig & Jones 1983).

In this paper, we present scanning Fabry-Pérot observations of the HH 7-11 flow system in the H $\alpha$  emission line.

---

Send offprint requests to: T.A. Movsessian

<sup>\*</sup> Based on observations taken at the 2.6 meter telescope of Byurakan Astrophysical Observatory, Armenia

## 2. Observations and data reduction

The observations were carried out at the 2.6-m telescope of Byurakan Observatory on 20 November 1997, with the ByuFOSC (Byurakan Faint Object Spectral Camera) in the interferometric mode, attached at the prime focus of the telescope. This device, as well as the pointing-guiding system “Bonneterre” were designed and assembled at Marseille Observatory in 1996. ByuFOSC includes a focal reducer (bringing the original F/4 focal ratio of the prime focus to F/2) with parallel beam allowing the installation of the various dispersing elements, filter wheel, and a CCD detector (Thomson 1028 × 1060 matrix with  $5e^-$  rms read-out noise and  $19\mu\text{m}$  pixel size). The scanning FP interferometer was placed in the parallel beam. The detector was used in half-obscured mode, allowing a quick shift of an exposed image to the obscured part of the matrix and the continuation of exposure of the next channel while reading out. This makes the scanning observations more effective because it minimizes the “dead time” between two exposures.

ByuFOSC is very similar to PALILA at CFHT (Amram et al. 1992) and CIGALE (Boulesteix et al. 1983). The instrument provides a useful field of  $6.5' \times 13'$  with one pixel equivalent to  $0.77''$  on the sky. The field was scanned through 24 steps, the exposure time was 420 s per channel, providing a total exposure time of 2h 48m. The quality of seeing was about  $2''$ . The  $H\alpha$  line was isolated with a narrow-band interference filter ( $\lambda=6563\text{\AA}$ ,  $\Delta\lambda=10\text{\AA}$ ). The FP interferometer was used in the 787 interference order, which gives  $R=10000$  at the  $H\alpha$  wavelength, with a free spectral range of  $376\text{ km s}^{-1}$  (or  $8.25\text{\AA}$ ) with sampling of  $0.34\text{\AA}$  per channel.

The data reduction procedure is an extension of the one used for the CIGALE instrument of Marseille Observatory (Laval et al. 1987), with some differences connected with the use of a CCD detector (Amram et al. 1992): due to the read-out noise, a CCD cannot read the image as frequently as an IPCS and so we make only a single exposure for each scanning step. To correct any variations in sky conditions during the exposure, we use the flux of the guiding star. Using calibration rings, obtained from the  $6598.95\text{\AA}$  neon emission line, we established a “phase map”, providing the wavelength calibration for each pixel. Areas surrounding the HH 7-11 system were used to subtract the background, consisting of  $H\alpha$  emission from NGC1333 and the  $H\alpha$  and OH geocoronal lines.

After obtaining the final wavelength cube, profiles of the  $H\alpha$  line for each pixel were extracted and the maps of the field in each wavelength step as well as in the integral  $H\alpha$  emission were produced.

## 3. Results

The whole system of HH 7-11 as it appears in the  $H\alpha$  emission line is presented in Fig. 1. This image is obtained as a sum of all spectral channels. The main HH knots as well as the SVS 13 source are prominent. Besides, some indications of the faint cone-like emission, which envelopes the outflow, can be traced. This emission cone is seen better in certain channels, as discussed below.

**Table 1.** Observed velocities and widths of the  $H\alpha$  emission line in the HH 7-11 complex

Object	Mean $V_{LSR}$ ( $\text{km s}^{-1}$ )	FWHM ( $\text{km s}^{-1}$ )
HH 7	-51	81
HH 8	-61	88
HH 9	-45	64
HH 10	-48	64
HH 11	-179	88
Bridge	-52	83

For the bridge only the area between HH 7 and HH 8, where it can be most clearly separated from the knots, was used.

The structure of the system as a whole and the shapes and the flux of different condensations strongly change with the velocity (Fig. 2). To make easier a comparison with the data of SB, all velocities in this paper are brought to the local standard of rest.

As can be readily seen, the HH 11 knot is prominent by its high velocity and compact star-like morphology. At lower velocities one can see other knots – HH 7–HH 10. At still lower velocities the entire group appears as well as the nebulous bridge connecting the individual knots. The triangular shape of HH 7 reveals itself better at even lower velocity. It is also noteworthy that the abovementioned nebulous cone becomes better defined at a velocity of about  $-51\text{ km s}^{-1}$  (see Fig. 2). Below we shall discuss each knot separately.

In Table 1 the mean parameters of the separate components of the HH 7-11 flow are given. They are obtained by integrating the profiles for each knot and between them. These data can be more or less directly compared with the data of SB, which, however, were obtained in a somewhat different way. The mean profiles themselves are shown in Fig. 3.

Mean profiles and radial velocities for all objects are quite similar to the SB data. The asymmetric profiles of HH 7 and HH 11 should be noted. Only for HH 8 is there a significant disagreement between our data and the velocities given by SB. In this object we observed a prominent velocity gradient (see below). We note a low FWHM of the HH-bridge from our measurements, contrary to SB, but one could not expect high precision in the measurements of such faint structures.

### 3.1. HH 7

On the image obtained by summation of all spectral channels, as well as on the previously obtained direct images, HH 7 appears as a triangular bow shock nebula, characterizing an outflow colliding with the ambient medium. As one can see from Fig. 4, where the images of HH 7 corresponding to the radial velocities  $-18$  and  $-125\text{ km s}^{-1}$  are superposed, in the brightest part of HH 7 we can distinguish two regions, clearly separated by their radial velocity. Spatial separation of these regions is about  $4''$ . This separation is the same as in the direct images in [SII] presented by Hartigan et al. (1989b). These structures could represent the bow shock and Mach-disk (the latter has a

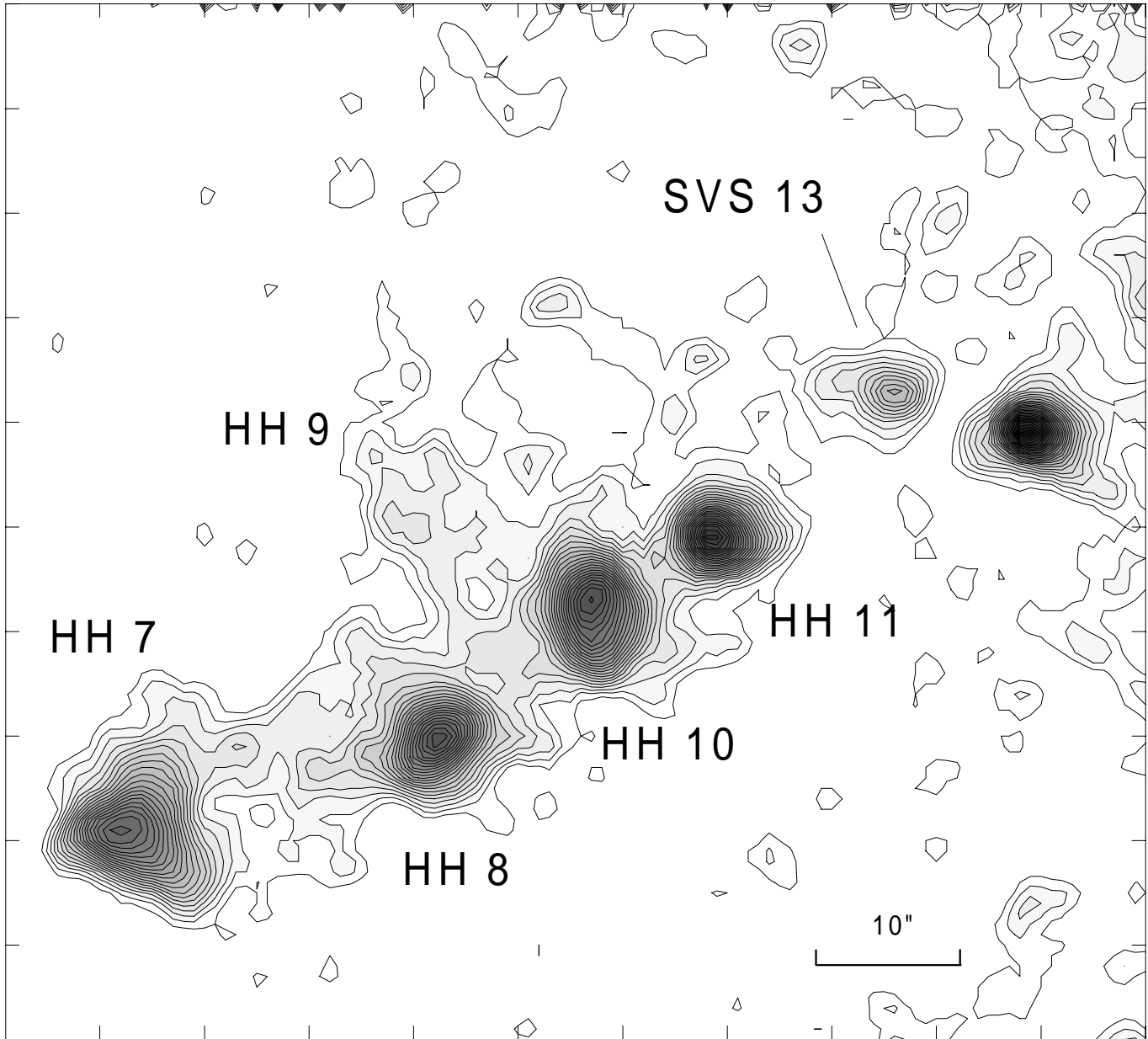


**Fig. 1.** Integrated monochromatic image of the HH 7-11 system in  $H\alpha$ . Full velocity range is from  $-264$  to  $+96$   $\text{km s}^{-1}$

much higher excitation level) of HH 7, as already noted by Hartigan et al. (1989b). The velocity gradient in HH 7 was found previously by SB, but here we can see the full morphology of the object at different velocities. We do not actually see a split  $H\alpha$  line in the area of HH 7, but various appearances of the object in the different spectral channels could be considered as the various contributions of both regions in the wings of the line profile. Thus, we can conclude that the bow shock has the lower velocity and the Mach-disk – the higher one; the Mach disk is spatially and kinematically distinct from the bow shock. This result is very similar to the result of FP spectrophotometry of HH 34 (Morse et al. 1992) and HH 111 (Morse et al. 1993) and suggesting the case of a “heavy” jet or bullet.

### 3.2. HH 8

This condensation is elongated along the flow. Its SW edge is sharper than other sides, which are connected with the nebulous bridge and faint emission arcs. As can be seen on direct images (SB, Hartigan et al. 1989b), it consists of two knots with different excitation as determined from the  $H\alpha/[S II]$  ratio (Hartigan et al. 1989b).

Our data show that the shape of the object markedly changes between  $-125$   $\text{km s}^{-1}$  and  $-18$   $\text{km s}^{-1}$ . This is an indication of the existence of several knots with various velocities inside the object. Indeed, we can clearly see three knots in the velocity field map of HH 8 (Fig. 5). The main elongated body of the object has a velocity gradient from  $-60$   $\text{km s}^{-1}$  in the NW

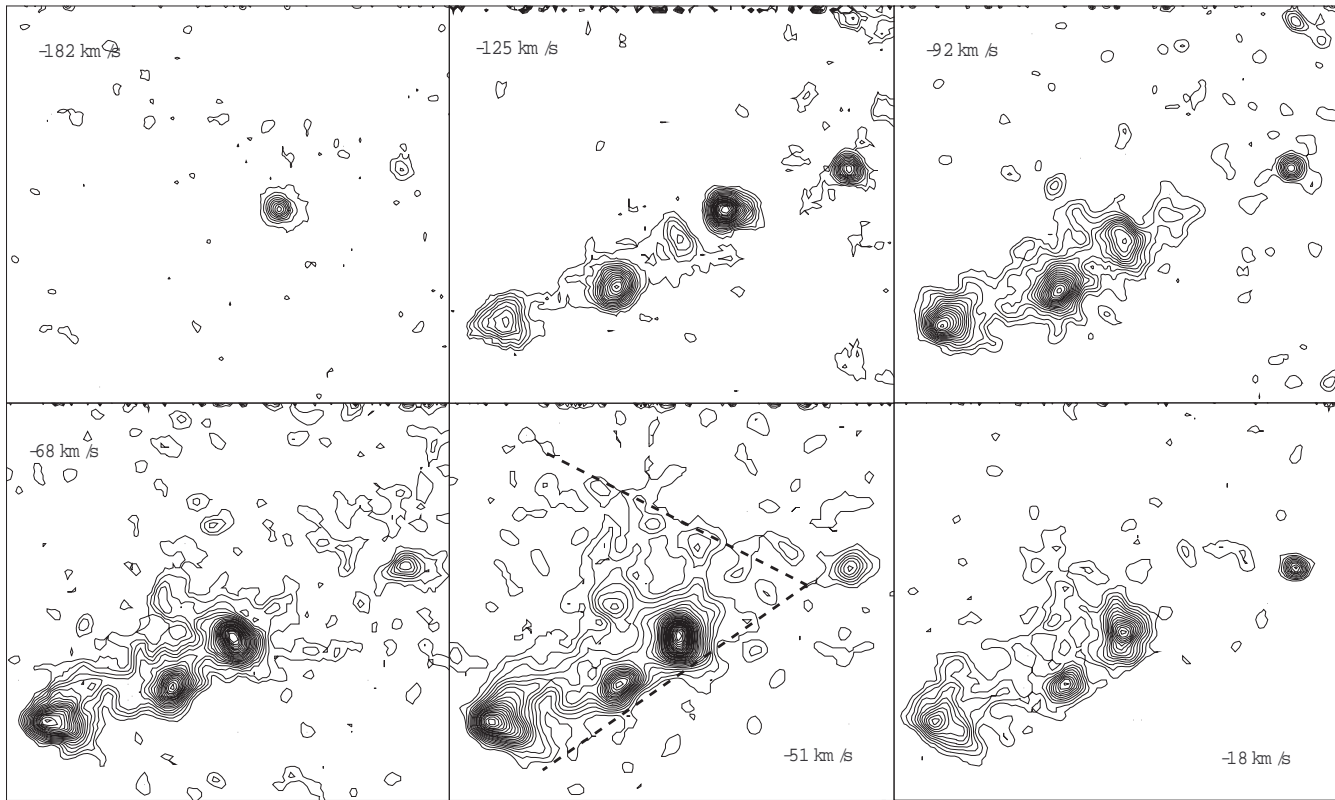


**Fig. 2.** Monochromatic images of the HH 7-11 system corresponding to various radial velocities. The edges of nebulous cone are shown by dashed lines on the frame corresponding to  $-51 \text{ km s}^{-1}$ .

part to  $-67 \text{ km s}^{-1}$  in the SE one. Besides, another spot with a distinctly different radial velocity up to  $-100 \text{ km s}^{-1}$  can be seen on the NE side of HH 8. The hints of its existence can also be found in the data of SB. By its location this spot lies inside the nebulous bridge and could not be separated on the narrow band filter images. Taking into account the existence of several spots with different radial velocities, the rather high FWHM for HH 8 is not surprising. It is highest ( $90 \text{ km s}^{-1}$  or even more) in the NW part of the object and drops to the  $84 \text{ km s}^{-1}$  in the SE part. In the high-velocity spot on the NE side it is even lower ( $76 \text{ km s}^{-1}$ ).

### 3.3. HH 9

HH 9 is not aligned with the other knots and also stands out because of its faintness. Its FWHM and mean velocity are similar to the nebulous bridge joining the knots. In the channels corresponding to the range from  $-100$  to  $-70 \text{ km s}^{-1}$ , HH 9 presents a clear bow-like shape and a connection with HH 10. At lower velocities it appears as an amorphous spot. The existence of another two faint knots, similar to HH 9 by their structure and kinematics and located near HH 8 should be noted (see below).

### 3.4. HH 10

HH 10 has been described as a double knot (SB, Hartigan et al. 1989b), elongated in the N-S direction. Its velocity and FWHM

are low and exceed only the values for HH 9. Several authors consider it as a mirror-like counterpart to HH 7, judging from its velocity field and from the lack of nebulosity between HH 10 and HH 11. Our data, however, do not show any well-defined velocity gradients in HH 10, even if some variations in radial velocities certainly exist from pixel to pixel. It should be mentioned that, according to the data presented by SB, changes in velocity in HH 10 are more obvious in  $[\text{S II}]$  emission than in  $\text{H}\alpha$ . At high velocities (see e.g. image for  $-125 \text{ km s}^{-1}$  on Fig. 2) at the place of HH 10 one can see a very interesting elongated and slightly curved feature. At lower velocities HH 10 splits into two bright and well-defined knots, separated by  $4.5''$ , exactly corresponding to its image in Fig. 1 of the SB paper. At still lower velocities ( $-68 \text{ km s}^{-1}$ ) the nebular bridge can be discerned, which connects HH 10 with HH 9 and HH 8 and also shows appendages in the direction of HH 11. Thus, some faint extended emission definitely exists (Fig. 2, see also Fig. 8) between HH 10 and HH 11, contrary to previous findings.

### 3.5. HH 11

More than once it was stressed by various authors, that this condensation differs from the other knots in this system by its high velocity and compactness. We confirm the suggestion of SB that the radial velocity is highest near the center of HH 11 (though not coinciding with the photocenter) and decreases to the edges (Fig. 6). We also confirm the changes in FWHM across

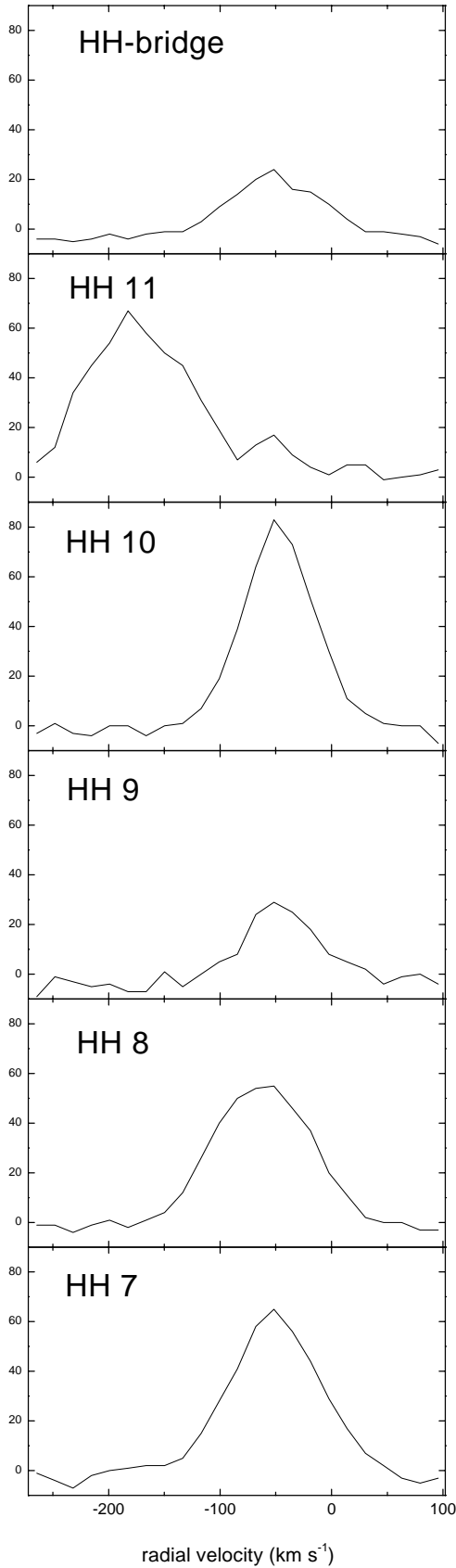


**Fig. 3.** Integrated profiles of the  $H\alpha$  emission line for the different condensations and the nebulous bridge.

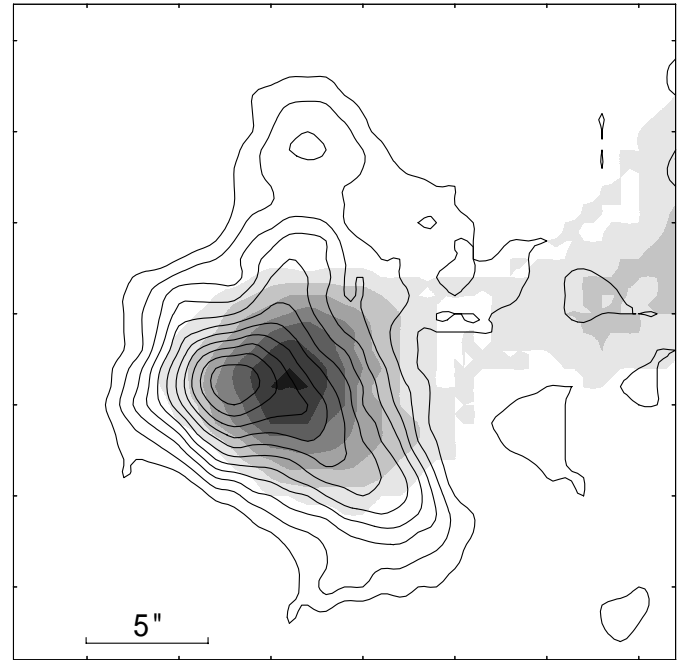


**Fig. 4.** Superposition of two monochromatic images of HH 7 corresponding to velocities of  $-125 \text{ km s}^{-1}$  (gray scale) and  $-18 \text{ km s}^{-1}$  (isolines).

the object: it seems that its value drops toward the edges along with the velocity. The location of the peak of velocity differs from the position suggested by SB, but their data are obtained for only a few points.

This also could be described in another way. HH 11, like the other knots in this flow, has different shapes at various wavelengths. In Fig. 7 we present the superposition of the HH 11 images, corresponding to the velocities  $-182$  and  $-117 \text{ km s}^{-1}$ . One can clearly see the triangular or even arcuate shape of HH 11 in the lower velocity. This result is similar to HH 7, but here high and low velocity regions nearly coincide. HH 11 is probably another working surface in the HH 7-11 complex, where the bow shock and Mach disk are spatially resolved.

### 3.6. HH bridge and “bubbles”

The well-defined knots of the HH 7-11 system are embedded in a faint emission envelope with a cone-like shape. Also some kind of a nebulous bridge connects all knots, which can be seen in Fig. 8. Contrary to the findings of SB and Hartigan et al. (1989b), we can trace it up to HH 11 and even further (detail “c” in Fig. 8). Its velocity does not differ much from the velocities of the knots. Its velocity dispersion is low, which is also inferred by its visibility only in a few channels.

Besides the bridge, we want to mention two interesting arcuate structures, also shown in Fig. 8 (details “a” and “b”), which are adjoined to it between HH 7 and HH 8, and which have some similarity with HH 9 in their morphology. The most interesting point is that they, along with all other arcuate structures found in this flow, are oriented in the same direction.

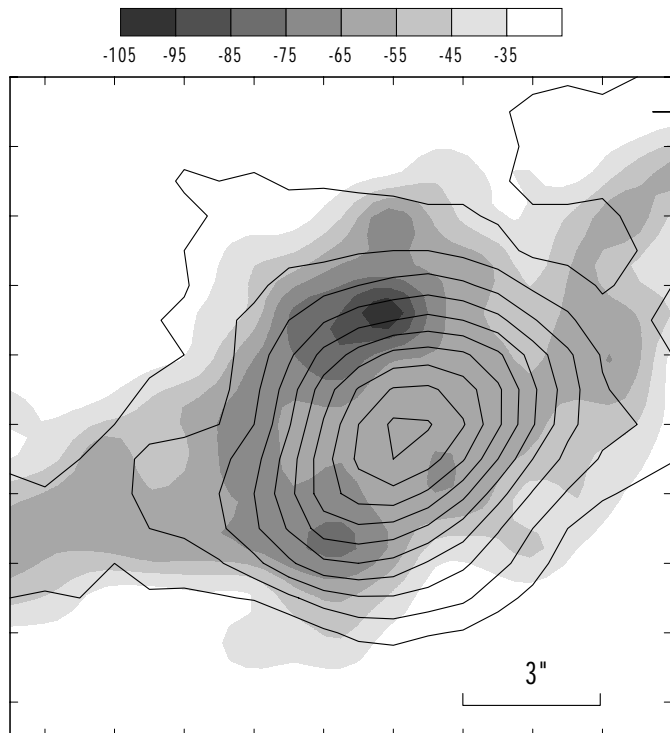


**Fig. 5.** The velocity field in HH 8 (gray scale) superposed on the integrated image of the object (isolines).

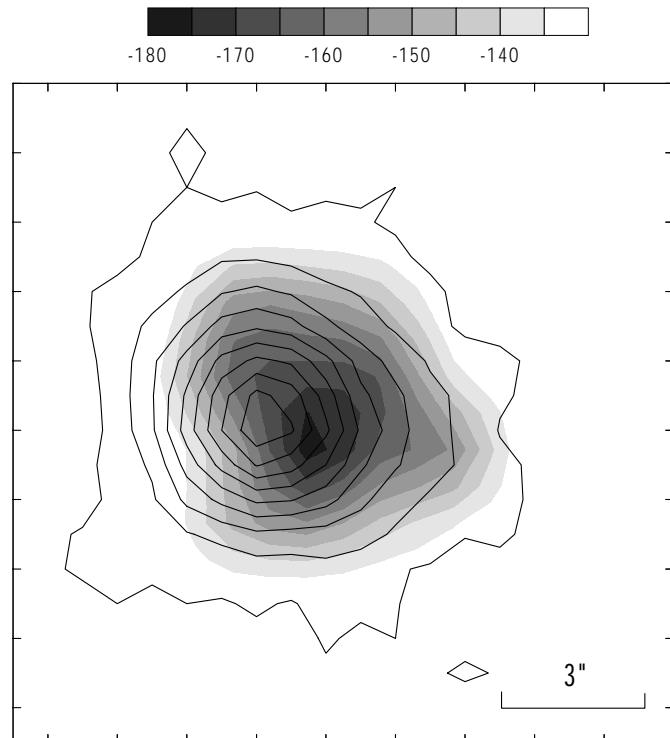


**Fig. 6.** The velocity field of HH 11 (gray scale) superposed on the integrated image of the object (isolines).

The opening angle of the faint cone is about 60 degrees and its apex falls in the field where SVS 13 and other sources are located. Thus, this cone could represent the cavity produced by the outflow.

#### 4. Discussion

The HH 7-11 flow always posed a problem for the theory of HH flows. Its several features, such as the combination of high velocities of knots with their very low excitation, or the fact that line profiles do not include zero velocity, are especially difficult to interpret. Some possible explanations were discussed in the paper of SB, where three different scenarios were considered: (a) an almost stationary flow; (b) a completely nonstationary combination of bullets and shocked cloudlets; and (c) an HH 34-like structure, where HH 11 was interpreted as a near-line-of-sight jet.

We support the idea that the large difference of the properties of HH 11 and the other HH-objects of this group could have fundamental importance for drawing a complete picture of this system. It is noteworthy that HH 11 was not detected in the emission of  $H_2$  (Hartigan et al. 1989b). In the more recent work of Everett (1997) HH 11 can be seen in the narrowband  $2.12 \mu\text{m}$  image as a small and rather faint spot, in contrast to its optical brightness. In the former paper it was suggested that preshock magnetic fields could be completely different in HH 11 and other knots of this group; thus, the difference is related not only to kinematics but also to the surrounding conditions. In all cases a fundamental problem for HH 11 still remains: the shock

velocity, determined from the line ratios and the predictions of shock models are always considerably lower than the “actual velocity”, determined from radial velocity and proper motion. Even if we take into account the standard explanation of this difference as the presence of a co-moving medium, it will be difficult to explain the low excitation of both HH 7 and HH 11, which have very dissimilar velocities, in the framework of a one-velocity moving medium.

Not going into details of the models, we want to point out yet another scenario. As noted above, the grouping of jets and HH-flows is not an uncommon phenomenon in active star-forming regions, of which NGC 1333 is one of the most active. The surroundings of HH 7-11 are very rich in different kinds of active sources and flows, discovered by optical, radio and infrared observations (Hodapp & Ladd 1995; Bachiller et al. 1998). On the other hand, the problem of the exact source of HH 7-11 flow is not solved yet. For a long time the probable source was SVS 13 (Strom et al. 1976), but on the basis of VLA observations another object, VLA 3 was suggested as a new source of HH 7-11 system (Rodríguez et al. 1997). Further investigations have revealed the double nature of SVS 13 (or VLA 4) as well as the elongation of VLA 3 in the direction of the HH 7-11 flow (Anglada et al. 2000). Besides, yet another radio source (Grossman et al. 1987) is located nearby. Taking into account all this, we suggest the possibility that the HH 7-11 complex consists of two independent flows from different sources. As can be seen from the above, there are plenty of possible identifications for these sources. This approach does not solve, of course, all the existing problems, but splits them into two parts.

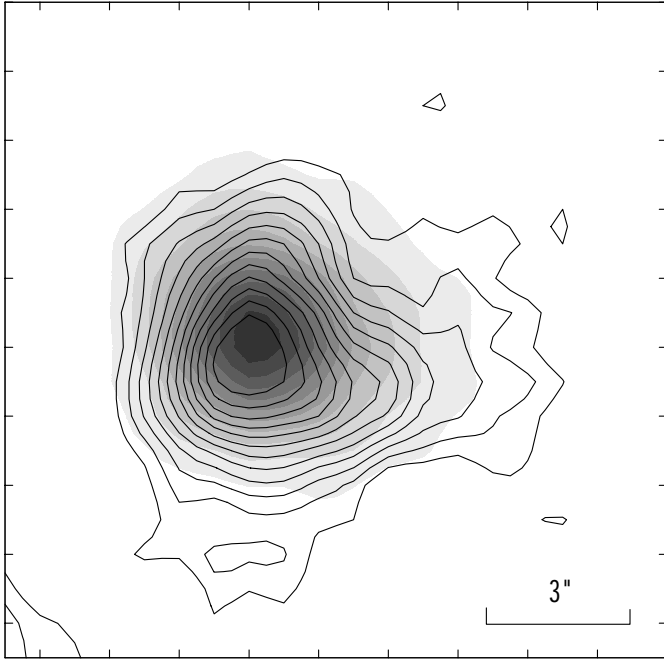


**Fig. 7.** Superposition of two monochromatic images of HH 11 corresponding to velocities  $-182 \text{ km s}^{-1}$  (gray scale) and  $-117 \text{ km s}^{-1}$  (isolines).

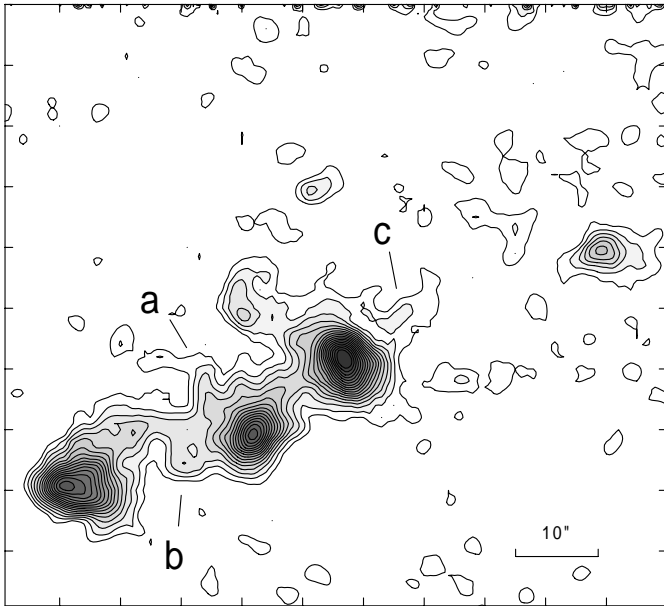


**Fig. 8.** Monochromatic image of system corresponding to  $-68 \text{ km s}^{-1}$ . Several structures, described in the text, are indicated

The first one of the flows is the HH 7-HH 10 system with relatively uniform kinematics, rather low electron densities and similar clumpy morphology in  $\text{H}\alpha$ ,  $[\text{S II}]$  and  $\text{H}_2$  as well. On the monochromatic images of this system, several curved structures are aligned in the same direction as the HH 7 bow shock. This morphology supports the idea that this system is a chain of shocks. The second one includes HH 11 which has a completely different morphology and also differs from the other knots by

its high velocity and appreciable proper motion. Its electron density is also higher. Besides, there are no detectable spatial separations between a bow shock and Mach disk for HH 11, while for HH 7 it is about  $4''$ . As another possible component of the second flow we want to mention the interesting and strange arcuate feature at the position of HH 10 with relatively high velocity, which is difficult to attribute to HH 10, but it could be considered as a bow shock connected with the second flow.

Another interesting feature of the HH 7-11 system, which remains still unexplained, is the nebular bridge. Taking into account the existence of the faint emission cone, on the southern side of which the main part of knots is located, we suggest that the bridge could represent the wall of this cone, additionally excited by oblique shocks. This idea is well supported by the results of  $\text{H}_2$  emission imaging (Everett 1997).

## 5. Conclusion

We have presented in this paper a kinematical and morphological study of the HH 7-11 complex using scanning FP data. Our main results are the following:

- We could kinematically separate the bow shock and Mach disk in HH 7 and HH 11. The bow shock is more developed at low velocities and the Mach disk at comparatively high ones. This result implies a “heavy” jet or bullet moving into a less dense ambient medium.
- We present the spatially resolved velocity field for the whole system as well as for separate condensations.
- The structure of the bridge and several arcuate structures was studied in more detail owing to the high contrast monochromatic images obtained with the FP scanning etalon.
- A new scenario with two separate flows from different sources has been suggested.

*Acknowledgements.* One of the authors (T.A.M.) wishes to thank the staff of Marseille Observatory for the help and hospitality during his stay. We also want to thank our referee Bo Reipurth for the critically reading the manuscript and many helpful comments.

## References

- Amram P., Le Coarer E., Marcellin M., et al., 1992, *A&AS* 94, 175  
 Anglada G., Rodriguez L.F., Torrelles J.M., 2000, *ApJ* in press  
 Bachiller R., Guilloteau S., Gueth F., et al., 1998, *A&A* 339, L49  
 Bally J., Devine D., Reipurth B., 1996, *ApJ* 473, L49  
 Blandford R.D., Rees M.J., 1974, *MNRAS* 169, 395  
 Blondin J.M., Königl A., Fryxell B.A., 1989, *ApJ* 337, L37  
 Böhm K.-H., Brugel E.W., Mannery E., 1980, *ApJ* 235, L137  
 Böhm K.-H., Brugel E.W., Olmsted E., 1983, *A&A* 125, 23  
 Boulesteix J., Georgelin Y.P., Marcellin M., Monnet G., 1983, *SPIE Conf. Instr. Astron.* V, 445, 37  
 Eisloffel J., Mundt R., 1997, *AJ* 114, 280  
 Everett M.E., 1997, *ApJ* 478, 246  
 Grossman E.N., Masson C.R., Sargent A.I., et al., 1987, *ApJ* 320, 356  
 Hartigan P., 1989a, *ApJ* 339, 987  
 Hartigan P., Curiel S., Raymond J., 1989b, *ApJ* 347, L31  
 Herbig G.H., 1974, *Lick Obs. Bull.* No.658  
 Herbig G.H., Jones B.F., 1983, *AJ* 88, 1040

- Hodapp K.-W., Ladd E.F., 1995, ApJ 453, 715
- Laval A., Boulesteix J., Georgelin Y.P., Georgelin Y.M., Marcelin M., 1987, A&A 175, 199
- Magakian T.Yu., Movsessian T.A., 1997, Astron. Rep. 41, 483
- Magakian T.Yu., Boulesteix J., Marcelin M., Le Coarer E., 1994, A&A 291, 928
- Molinari S., Noriega-Crespo A., Ceccarelli C., et al., 2000, ApJ in press
- Morse J.A., Hartigan P., Cecil G., Raymond J.C., Heathcote S., 1992, ApJ 399, 231
- Morse J.A., Heathcote S., Cecil G., Hartigan P., Raymond J.C., 1993, ApJ 410, 764
- Morse J.A., Hartigan P., Heathcote S., Raymond J.C., Cecil G., 1994, ApJ 425, 738
- Movsessian T.A., 1992, SvA Letters 18, 748
- Mundt R., Brugel E.W., Bührke T., 1987, ApJ 319, 275
- Mundt R., Ray T.P., Bührke T., Raga A.C., Solf J., 1990, A&A 232, 37
- Raga A., 1988, ApJ 335, 820
- Reipurth B., Heathcote S., 1991, A&A 246, 511
- Reipurth B., Heathcote S., 1992, A&A 257, 693
- Rodriguez L.F., Anglada G., Curiel S., 1997, ApJ 480, L125
- Solf J., Böhm K.-H., 1987, AJ 93, 1172 [SB]
- Strom S.E., Vrba F.J., Strom K.M., 1976, AJ 81, 314